Amoeba-Inspired Nanoarchitectonic Computing: Solving Intractable Computational Problems Using Nanoscale Photoexcitation Transfer Dynamics

Article *in* Langmuir · April 2013

DOI: 10.1021/la400301p · Source: PubMed

7 authors, including:

Masashi Aono
Tokyo Institute of Technology
64 PUBLICATIONS **596** CITATIONS
SEE PROFILE

Makoto Naruse
National Institute of Information and Comm…
170 PUBLICATIONS **956** CITATIONS
SEE PROFILE

Song-Ju Kim
National Institute for Materials Science
55 PUBLICATIONS **255** CITATIONS
SEE PROFILE

Hirokazu Hori
University of Yamanashi
96 PUBLICATIONS **919** CITATIONS
SEE PROFILE

Langmuir

Article

pubs.acs.org/Langmuir

Amoeba-Inspired Nanoarchitectonic Computing: Solving Intractable Computational Problems Using Nanoscale Photoexcitation Transfer Dynamics

Masashi Aono,*[,†] Makoto Naruse,[‡,§] Song-Ju Kim,[†] Masamitsu Wakabayashi,[⊥] Hirokazu Hori,[#] Motoichi Ohtsu,[§,∥] and Masahiko Hara[†]

[†]Flucto-Order Functions Research Team, RIKEN-HYU Collaboration Research Center, RIKEN Advanced Science Institute, 2-1 Hirosawa, Wako, Saitama 351-0198, Japan

[‡]Photonic Network Research Institute, National Institute of Information and Communications Technology, 4-2-1 Nukui-kita, Koganei, Tokyo 184-8795, Japan

[§]Nanophotonics Research Center and [∥]Department of Electrical Engineering and Information Systems, Graduate School of Engineering, The University of Tokyo, Japan

[⊥]Department of Biomolecular Engineering, Tokyo Institute of Technology, 4259 Nagatsuta, Midori-ku, Yokohama 226-8501, Japan

[#]Interdisciplinary Graduate School of Medicine and Engineering, University of Yamanashi, Takeda 4-3-11, Kofu, Yamanashi 400-8511, Japan

ABSTRACT: Biologically inspired computing devices and architectures are expected to overcome the limitations of conventional technologies in terms of solving computationally demanding problems, adapting to complex environments, reducing energy consumption, and so on. We previously demonstrated that a primitive single-celled amoeba (a plasmodial slime mold), which exhibits complex spatiotemporal oscillatory dynamics and sophisticated computing capabilities, can be used to search for a solution to a very hard combinatorial optimization problem. We successfully extracted the essential spatiotemporal dynamics by which the amoeba solves the problem. This amoeba-inspired computing paradigm can be implemented by various physical systems that exhibit suitable spatiotemporal dynamics resembling the amoeba's problem-solving process. In this Article, we demonstrate that photoexcitation transfer phenomena in certain quantum nanostructures mediated by optical near-field interactions generate the amoebalike spatiotemporal dynamics and can be used to solve the satisfiability problem (SAT), which is the problem of judging whether a given logical proposition (a Boolean formula) is self-consistent. SAT is related to diverse application problems in artificial intelligence, information security, and bioinformatics and is a crucially important nondeterministic polynomial time (NP)-complete problem, which is believed to become intractable for conventional digital computers when the problem size increases. We show that our amoeba-inspired computing paradigm dramatically outperforms a conventional stochastic search method. These results indicate the potential for developing highly versatile nanoarchitectonic computers that realize powerful solution searching with low energy consumption.

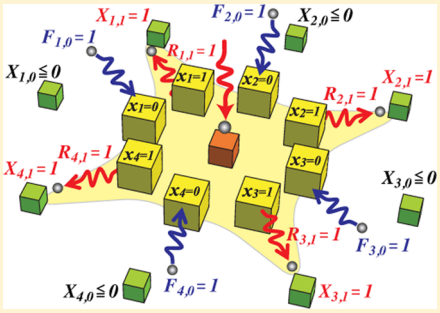

INTRODUCTION

Biological systems can be regarded as powerful computers in which massive numbers of elements such as biopolymers, proteins, and cells interact with each other and process vast amounts of environmental information in a self-organized manner.[1] For example, chains of amino acids promptly solve the protein folding problem, which is believed to be impossible for conventional digital computers to solve in a practical polynomial time.[2] For such an intractable problem, the number of all solution candidates, which should be examined thoroughly, grows exponentially as a function of the problem size and reaches an astronomical number, causing a combinatorial explosion.[3] What could be the source of the tremendous computational powers of biological systems? We believe that a key would be interactions among the elements.[1] More specifically, the interactions, which involve dynamic instabilities such as oscillations and fluctuations and physical constraints such as conservation laws of several resources, would generate complex spatiotemporal dynamics that could explore a state space broadly and efficiently. Learning how interacting biological elements perform powerful computations will provide insightful role models for promoting nanoarchitectonics, which aims to exploit novel functionalities using interacting nanoscale elements.

Natural computing is an emerging research field that uses the knowledge obtained from various natural phenomena, includ-

Special Issue: Interfacial Nanoarchitectonics

Received: January 22, 2013
Revised: March 22, 2013

   dx.doi.org/10.1021/la400301p | *Langmuir* XXXX, XXX, XXX–XXX

ing biological processes, to complement and overcome the limitations of conventional digital computers in solving computationally demanding problems in a decentralized manner, making optimal decisions adaptively in uncertain environments, reducing energy consumption, and so on.[4,5] Several algorithms for solving computationally demanding problems have been abstracted from biological processes such as information processing in neural networks,[6] evolutionary processes in genetic systems,[7] optimal path finding by ants,[8] and optimal solution search by swarms of insects.[9] In this context, a single-celled amoeboid organism, a plasmodium of the true slime mold *Physarum polycephalum* (Figure 1a), has been actively investigated owing to its intriguing computational capabilities. For example, this amoeba, despite the absence of a central nervous system, connects the optimal routes among food sources by changing its amorphous shape.[10,11] These computational capabilities were expected to emerge from its complex spatiotemporal behavior in which the volume of each part oscillates with a period of approximately 1 to 2 min in a fluctuating manner.[12,13]

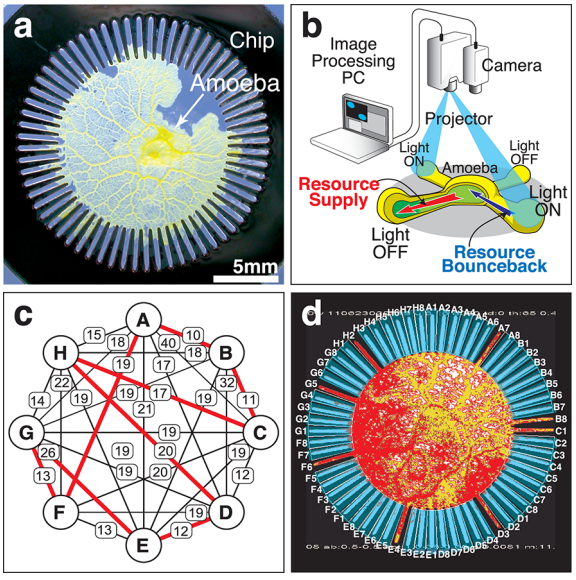

Figure 1. Amoeba-based computing. (a) Amoeboid organism *P. polycephalum* and Au-coated 64-lane chip resting on a nutrient-rich agar plate. The amoeba remains inside the chip because of its attraction to nutrients in the plate and its aversion to metal. (b) Experimental setup. The image of the amoeba recorded by a video camera was processed using a PC to update the image pattern for illumination with a projector. (c) Example of the eight-city map in the traveling salesman problem. The distance between each pair of cities is indicated on the corresponding edge. There uniquely exist shortest and longest routes having lengths of 100 and 200, respectively, where the average route length for all possible 2520 solutions was 149.1. (d) High-quality solution found by the amoeba-based computer. The amoeba's shape represents the route CHDEGFABC with a length of 128 (the red unicursal line in c), which is evaluated as being in the top 10% of solutions with regard to quality (shortness). Each lane of the chip is labeled *Vk*, which indicates the city name *V* and its visiting order *k*. Red and yellow pixels indicate increasing and decreasing thicknesses, respectively. Blue trapezoids indicate illuminated regions.

Aono et al. devised an amoeba-based computer (ABC)[14,15] that incorporates an amoeba to solve various optimization problems. In the ABC, we harnessed complex spatiotemporal oscillatory dynamics of the amoeba in a multilane chip (Figure 1a) by introducing unique optical feedback control (Figure 1b), which we call bounceback control. Under normal conditions, the amoeba supplies its intracellular resource (protoplasm) to its pseudopod-like branches so that they elongate by repeating several cycles of oscillations while conserving the total volume of the entire body. However, the branches retreat when stimulated by visible light as the resource bounces back from the illuminated region owing to the photoavoidance response. Sharing the constant volume of the resource, these branches interact with each other by transmitting information on their stimulated experiences through exchanging the resource to make an optimal decision on resource allocation. In the ABC, we updated the light stimulation of all of the lanes at 6 s intervals, depending on the change in the amoeba's shape. Under this dynamic environment, the organism tried to deform into an optimal shape, maximizing the body area for maximal nutrient absorption while minimizing the risk of being exposed to light stimuli.

We designed a rule for updating the light stimulation based on certain recurrent neural network dynamics so that the amoeba could search for a solution to the traveling salesman problem (TSP).[16] The TSP, one of the best-studied intractable problems, is stated as follows: given a map of n cities that defines the travel distance from any city to any other city (Figure 1c), find the shortest route for visiting each city exactly once and returning to the starting city. In the ABC, the challenge for the amoeba to find the shortest route is that its branches should not enter frequently illuminated lanes and should elongate into the optimal combination of the least frequently illuminated lanes. Note that the optimal combination cannot be found if this organism always obeys the optical feedback control rule. To compare the route lengths of solution candidates, it is necessary for the amoeba to make "errors" at appropriate frequencies. That is, to explore the state space broadly, sometimes the organism needs to misallocate the resource to its branches, contrary to their normal photoavoidance response, so that the branches expand even when illuminated and shrink even when unilluminated. In reality, owing to the intrinsic spatiotemporal oscillatory dynamics, each branch could vary its responses to light stimuli suitably depending on its oscillation phase, so the amoeba could find a high-quality solution through trial and error, as shown in Figure 1d.[17]

We evaluated the computational performance of the ABC by increasing the problem size n from 4 to 8 to explore how the explosive growth in the number of solutions $[(n-1)!/2 = 3, 12, 60, 360,$ and $2520]$ affects the performance.[18] Interestingly, the ABC found a high-quality solution (a shorter route) with a high probability and robustly maintained the high quality independently of n. Moreover, the search time required to find the solution grew almost linearly as a function of n, despite the explosive expansion of the state space. These results suggested that the ABC has an economical search ability to find a satisfactory high-quality solution at a low exploration cost, including a short search time. This might be a strategy of this organism to survive adaptively in uncertain environments.

Extracting the essential factors from the amoeba's economical search process, Aono et al. formulated an amoeba-inspired computing paradigm as a hybrid process of two spatiotemporal dynamics that are counterparts of the shape-changing behavior of the amoeba and the illumination-updating rule of the optical feedback control.[19] The former dynamics, which allocate the resource so that it is supplied to nonstimulated units and is

dx.doi.org/10.1021/la400301p | *Langmuir* XXXX, XXX, XXX–XXX

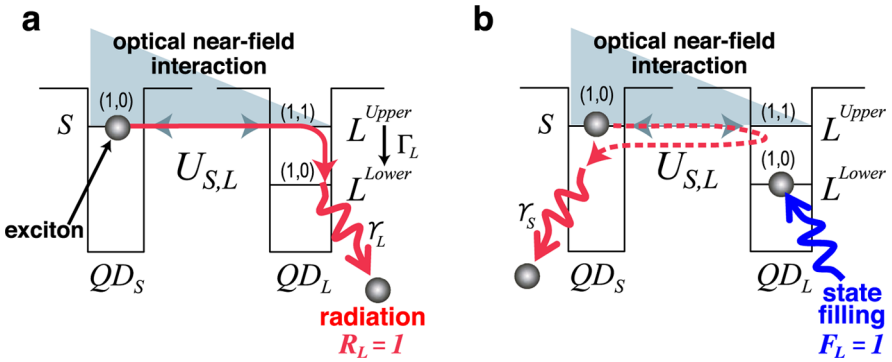

Figure 2. Photoexcitation transfer between QDs. (a) Exciton in QD_S is transferred to QD_L, from which it subsequently radiates. (b) Exciton population bounced back from QD_L when the lower energy level, L^{lower}, is filled with another exciton.

bounced back from stimulated units, must generate appropriate fluctuations in the stimulus response to make errors at optimal frequencies. In addition, the latter dynamics, which we call the bounceback control dynamics, should update the stimulations depending on the former states and should adequately apply repulsive stimulation to unfavorable units from which the resource should be bounced back.

These observations imply that, to develop novel computing devices that operate much faster than the amoeba, it would be possible to use the stimulus-responsive spatiotemporal dynamics of various physical systems in which some resource of the system is transferred to its subsystems in a fluctuating manner.

In fact, Naruse et al. showed that the spatiotemporal dynamics of photoexcitation transfer between quantum mechanical electronic states (excitonic states), which are implemented in semiconductor nanostructures and are mediated by optical near-field interactions, could be used to solve constraint satisfaction problems.[20,21] Optical near-field interactions occur at scales far below the wavelength of light and enable photoexcitation transfer to dipole-forbidden energy levels, which cannot be realized by conventional optical far fields. A useful theoretical treatment of the near-field optical excitation transfer process has been established on the basis of the dressed-photon model,[22] and the process has been experimentally demonstrated in quantum dot (QD) systems based on various semiconductors such as InGaAs,[23] ZnO,[24] and CdSe.[25] Kawazoe et al. demonstrated room-temperature photoexcitation transfer using two layers of 2D-ordered InGaAs QDs.[26] Akahane et al. fabricated 60 highly stacked layers of InAs QDs and produced a system with a total QD density of $4.73 \times 10^{12}/\mathrm{cm}^2$.[27] Moreover, Naruse et al. showed that the minimum energy dissipation in photoexcitation transfer has been shown to be 10^4 less than that required for a bit flip in a CMOS logic gate in conventional electrically wired devices.[28] These facts suggest that, by exploiting these photoexcitation transfer dynamics, our amoeba-inspired computing paradigm can be implemented on highly integrated low-energy-use quantum nanostructures.

Our paradigm is applied to solving the satisfiability problem (SAT), which is one of the most important intractable problems in computer science. In computational complexity theory, the complexity class NP (nondeterministic polynomial time) includes many difficult problems in which no polynomial time algorithm has been found so far. That is, these difficult problems often require an exponential time for conventionally known algorithms to solve. SAT was the first problem shown to be NP-complete, that is, the most difficult problem among those that belong to the class NP.[3] The NP completeness implies that all NP problems, including thousands of practical real-world problems, can be reduced to SAT. A powerful SAT solver, therefore, has enormous versatility. In fact, it is applied to a wide range of application problems such as software and hardware design, planning, constraint optimization, automatic inference, cryptography, and protein structure prediction.

In this Article, we first introduce the photoexcitation transfer dynamics, review the satisfiability problem, and describe our newly developed computing paradigm. Then, we compare the performance of our paradigm with that of a well-known algorithm. Finally, we discuss the origin of our paradigm's high performance and conclude the Article.

EXPERIMENTAL SECTION

Photoexcitation Transfer between Quantum Dots. We assume two spherical QDs whose radii are r_S and r_L ($>r_S$), which we call a small QD (QD_S) and a large QD (QD_L), respectively, as shown in Figure 2a. Under irradiation by input light, an exciton (electron–hole pair) is generated in QD_S. We consider photoexcitation transfer phenomena between QD_S and QD_L (i.e., transitions of exciton to states specified by (q_1, q_2), where q_1 and q_2 are the orbital angular momentum quantum number and magnetic quantum number, respectively). The energy eigenvalues of the states are given by

$$E_{(q_1,q_2)} = E_g + E_{ex} + \frac{\hbar^2 \alpha_{(q_1,q_2)}^{\ 2}}{2mr^2} (q_1 = 1, 2, 3, \ldots) \quad (1)$$

where E_g is the band gap energy of the bulk semiconductor, E_{ex} is the exciton binding energy in the bulk system, m is the effective mass of the exciton, and $\alpha_{(q_1,q_2)}$ are determined from the boundary conditions, for example, $\alpha_{(q_1,0)} = q_1\pi$, $\alpha_{(1,1)} = 4.49$.

According to eq 1, there exists a resonance between the level with quantum number (1, 0) in QD_S, denoted by S in Figure 2a, and that with quantum number (1, 1) in QD_L, denoted by L^{upper}, if $r_L/r_S = 4.49/\pi \approx 1.43$. These energy levels S and L^{upper} are in resonance with each other and are connected by an interdot optical near-field interaction, $U_{S,L}$, which is given by a Yukawa-type potential

$$U_{S,L} = \frac{\nu \exp(-\mu \mathrm{dst}(S, L))}{\mathrm{dst}(S, L)} \quad (2)$$

where $\mathrm{dst}(S, L)$ denotes the distance between QD_S and QD_L and ν and μ are constants.[22,29] Note that, in typical light–matter interactions via optical far fields, transitions to states specified by $(q_1, q_2) = (1, 1)$ are not allowed because this is a dipole-forbidden energy level. However, in optical near-field interactions, because of the large spatial inhomogeneity of the localized optical near fields at the surface of nanoscale materials, L^{upper} is allowed to be populated by excitons,

dx.doi.org/10.1021/la400301p | Langmuir XXXX, XXX, XXX–XXX

violating the conventional optical selection rules.[29] Therefore, the exciton at level S in QD_S could be transferred to level L^{upper} in QD_L.

In QD_L, because of the sublevel energy relaxation with a relaxation constant Γ_L, which is faster than the optical near-field interaction, the exciton relaxes to the (1, 0) level, denoted by L^{lower}, from where it radiatively dissipates (Figure 2a). In addition, because the radiation lifetime of QDs is inversely proportional to their volume,[30] finally we find "unidirectional" exciton transfer from QD_S to QD_L. We consider that the exciton is transferred from QD_S to QD_L when we observe light emission from QD_L due to the radiation of optical energy. The radiation from L^{lower} is represented by the relaxation constant γ_L.

The unidirectionality of exciton transfer originates from the energy dissipation occurring in QD_L. Therefore, by disturbing the sublevel energy relaxation in QD_L, we can block exciton transfer to QD_L. In fact, when the lower energy level L^{lower} of QD_L is filled with another exciton, the exciton in QD_S cannot move to QD_L. The blocked exciton will bounce back and forth between QD_L and QD_S (optical nutation) and will finally dissipate from QD_S according to the relaxation constant γ_S, as shown schematically in Figure 2b. We can fill the state L^{lower} of QD_L by light stimulation, which is referred to as state filling. Like the branch of the amoeba that shrinks when illuminated, the probability of exciton transfer to QD_L is reduced when it is state-filled, as described in the next section.

Spatiotemporal Dynamics of Photoexcitation Transfer. To implement the amoeba-inspired computing paradigm, we design a system where a QD_S is surrounded by a number of QD_L's, as shown in Figure 3a. For simplicity, we consider four QD_L's (QD_A, QD_B, QD_C, and QD_D), each of which has the same upper level, lower level, sublevel relaxation constant, and radiation constant L^{upper}, L^{lower}, Γ_L, and γ_L, respectively.

We describe the basic properties of the spatiotemporal dynamics of exciton transfer in this system. We assume that the system initially has one exciton in S. For each QD_L, through the interdot interaction $U_{S,L}$, the exciton in S could be transferred to L^{upper}. Accordingly, we can derive quantum master equations in the density matrix formalism.[29,31] The interaction Hamiltonian is given by

$$H_{int} = \begin{pmatrix} 0 & U_{S,A} & U_{S,B} & U_{S,C} & U_{S,D} \\ U_{S,A} & 0 & 0 & 0 & 0 \\ U_{S,B} & 0 & 0 & 0 & 0 \\ U_{S,C} & 0 & 0 & 0 & 0 \\ U_{S,D} & 0 & 0 & 0 & 0 \end{pmatrix} \quad (3)$$

Although interactions between the QD_L's occur, for simplicity they are not considered here. The relaxation regarding the above-mentioned states is described by $N_\Gamma = \mathrm{diag}(\gamma_S, \Gamma_A, \Gamma_B, \Gamma_C, \Gamma_D)$. Then the Liouville equation for the system is

$$\frac{d\rho(t)}{dt} = -\frac{i}{\hbar}[H_{int}, \rho(t)] - N_\Gamma \rho(t) - \rho(t) N_\Gamma \quad (4)$$

where $\rho(t)$ is the density matrix with respect to the five energy levels and $\hbar$ is Planck's constant divided by 2π. Similarly, we can derive ordinary differential equations with respect to L^{lower}, which is populated by the relaxations from L^{upper} with constants Γ_L, which decay radiatively with relaxation constants γ_L.

In the numerical calculation, we assume ${U_{S,L}}^{-1}$ = 100 ps, ${\Gamma_L}^{-1}$ = 1 ps, ${\gamma_L}^{-1}$ = 1 ns, and ${\gamma_L}^{-1} = (r_L/r_S)^3 \times {\gamma_L}^{-1} \approx 2.92$ ns as a typical parameter set. For instance, in experimental demonstrations based on a CdSe/ZnS core−shell QD,[32] the measured radiation lifetime of a CdSe/ZnS QD with a diameter of 2.8 nm (QD_L) was 2.1 ns, which is close to the radiation lifetimes ${\gamma_L}^{-1}$ and ${\gamma_S}^{-1}$. In addition, the interaction time between QD_S and QD_L was estimated to be 135 ps,[32] which is also close to the above interdot interaction time ${U_{S,L}}^{-1}$.

When the above Liouville equation is solved numerically (eq 4), the time evolution of the populations of the lower energy levels of the QD_L's, which are relevant to occurrences of radiation, can be calculated. Figure 3b indicates that the system uniformly grows the

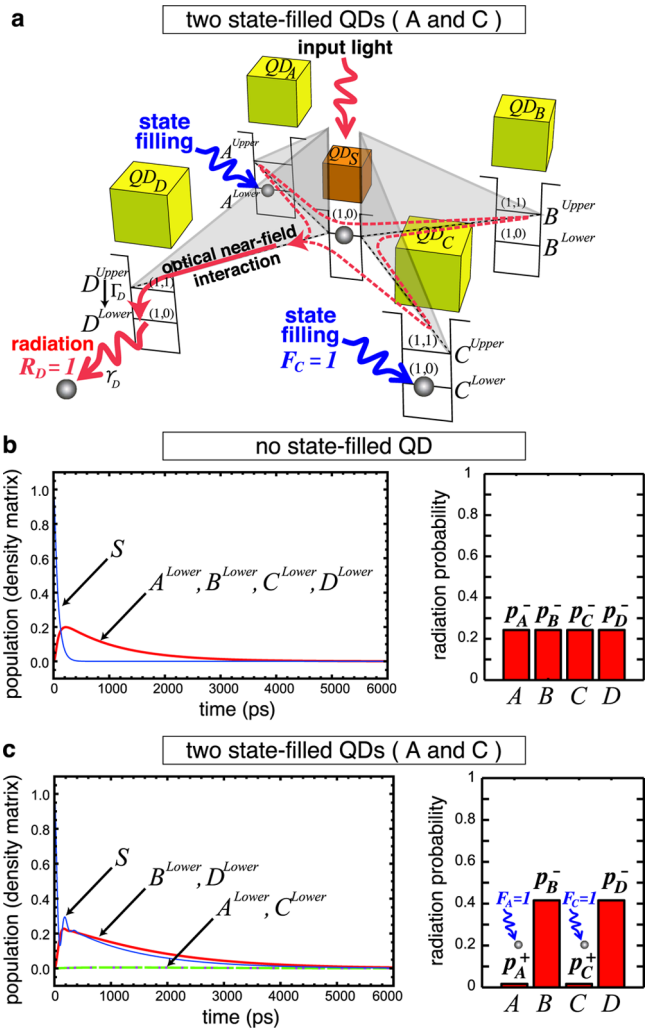

Figure 3. Spatiotemporal dynamics of photoexcitation transfer in the system with QD_S surrounded by four large QDs (QD_A, QD_B, QD_C, and QD_D). (a, c) When QD_A and QD_C are state-filled, the exciton is likely to be transferred to either QD_B or QD_D, from which it radiates. Each of radiation probabilities (right panel) is calculated as a time integration of each corresponding time evolution of populations (left panel) divided by a gain constant g. (b) In the absence of state-filling stimulation, radiation occurs in the four large dots with equal probability.

populations of A^{lower}, B^{lower}, C^{lower}, and D^{lower} while reducing the population of S and finally reaches equilibrium. Figure 3c shows the case where QD_A and QD_C are subjected to state filling by light stimulation. A way of describing such a state-filling effect in eq 4 is to induce a significant increase in the sublevel relaxation lifetime of the state-filled QD_A and QD_C; we assume that the lifetime increased to ${\Gamma_A}^{-1} = {\Gamma_C}^{-1} = 10^5$ ps. Such a formation has been validated in the literature.[21] Because of these changes in the parameters, the exciton is more likely be transferred to QD_B or QD_D than to QD_A or QD_C, as shown in Figure 3c.

Radiation Probability. We can obtain the probability p_L that the exciton in QD_S is transferred to QD_L, from which it subsequently radiates by numerically integrating the time evolution of the population of L_{lower} over 6000 ps and dividing it by a certain gain constant g, as shown in Figure 3b,c. In our numerical calculation, we assume that radiation occurs in QD_L if a uniformly generated random number in [0.0, 1.0] is less than the value of p_L. Therefore, p_L represents the probability that radiation from QD_L is observed within 6000 ps. Thus, more than one radiation event can occur in a number of QD_L's. This verifies that $p_A + p_B + p_C + p_D \neq 1$. The radiation

dx.doi.org/10.1021/la400301p | Langmuir XXXX, XXX, XXX−XXX

probabilities when QD_L is state-filled and non-state-filled are denoted by p_L^+ and p_L^-, respectively.

We briefly discuss the similarities between the photoexcitation transfer dynamics and the shape-changing behavior of the amoeba. We consider that the amoeba's intracellular resource supply to its branch can be compared to exciton transfer to QD_L (i.e., radiation in QD_L). As the amoeba's intracellular resource is bounced back from illuminated branches, the exciton population is bounced back from state-filled QD_L's. However, as mentioned previously, to explore the state space broadly, the amoeba had to make errors at appropriate frequencies; the branch varied its normal photoavoidance response depending on its intrinsic oscillation phase so that it could expand even when illuminated and shrink even when unilluminated. In the photoexcitation transfer dynamics, these error mechanisms are implemented by the occurrence and nonoccurrence of radiation in state-filled and non-state-filled QD_L's with probabilities of p_L^+ and $1 - p_L^-$, respectively.

As shown in the right panels of Figure 3b,c, p_A and p_C decreased owing to state-filling stimulation, whereas p_B^- and p_D^- increased as if they tried to compensate for the decrements in p_A and p_C. That is, the radiation probability of each QD_L varies in response to the current state-filling stimulation applied to other distant QD_L's. In other words, the stimulus response of each QD_L is not determined locally. This nonlocal property is shown more clearly in Figure 4a,b. The radiation

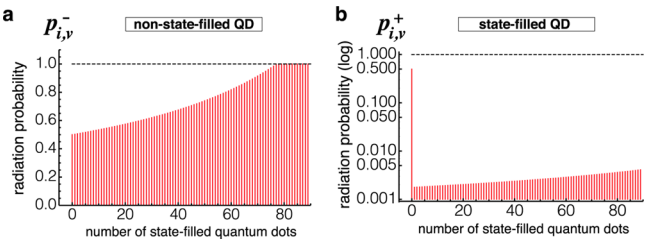

Figure 4. Dependence of the radiation probability on the number of all state-filled $QD_{j,u}$'s, $f = \Sigma_{j,u}F_{j,u}(t)$, in the system consisting of 150 $QD_{j,u}$'s for solving a 75-variable SAT. (a) Radiation probability $p_{i,v}^-$ in non-state-filled $QD_{i,v}$. (b) Radiation probability $p_{i,v}^+$ in state-filled $QD_{i,v}$. Each probability, which is obtained as a time integration of population evolution divided by g, grows nonlinearly as a function of f. We set g such that it gives $p_{i,v}^- = p_{i,v}^+ = 0.5$ when $f = 0$.

probabilities of non-state-filled and state-filled QD_L's, p_L^- and p_L^+, increased nonlinearly as a function of the number of all state-filled QD_L's. In case of the amoeba, the previously mentioned conservation law in the total resource volume entailed a nonlocal correlation among the amoeba's branches (i.e., a volume increment in one branch is immediately compensated for by a volume decrement(s) in the other branch(es)). This nonlocal correlation was shown to be useful for efficient and adaptive decision making.[33]

Satisfiability Problem. SAT is the problem of determining if a given Boolean formula ϕ of N variables $x_i \in \{0 \text{ (false)}, 1 \text{ (true)}\}$ ($i \in I = \{1, 2,..., N\}$) is satisfiable (i.e., there exists at least one assignment of truth values (0 or 1) to the variables that makes the formula true ($\phi = 1$)). Roughly speaking, ϕ represents a logical proposition, and the existence of a satisfying assignment verifies that the proposition is self-consistent. For example, a formula $\phi_{ex} = (x_1 \vee \neg x_2) \wedge (\neg x_2 \vee x_3 \vee \neg x_4) \wedge (x_1 \vee x_3) \wedge (x_2 \vee \neg x_3) \wedge (x_3 \vee \neg x_4) \vee (\neg x_1 \vee x_4)$ has a satisfying assignment $(x_1, x_2, x_3, x_4) = (1, 1, 1, 1)$, which is a uniquely existing solution. Even if ϕ has more than one solution, this instance can be solved when at least one solution is found. However, to prove unsatisfiability, the only sure method known to be applicable to arbitrary formulas is to check the inconsistency of all possible assignments, the number of which grows exponentially as 2^N.

SAT is called 3-SAT when ϕ consists of M clauses that are connected by $\wedge$ (and), and each clause connects at most three literals by $\vee$ (or) as $(x_j^* \vee x_k^* \vee x_l^*)$, where each literal x_i^* can be either x_i or $\neg x_i$. Any SAT instance can be transformed to a 3-SAT instance, and 3-SAT is also NP-complete. In this study, we design our computing paradigm for application to solving 3-SAT.

Amoeba-Inspired Nanoarchitectonic Computer. As shown in Figure 5, to solve an N-variable 3-SAT, we use $2N$ large QDs ($QD_{i,v}$'s)

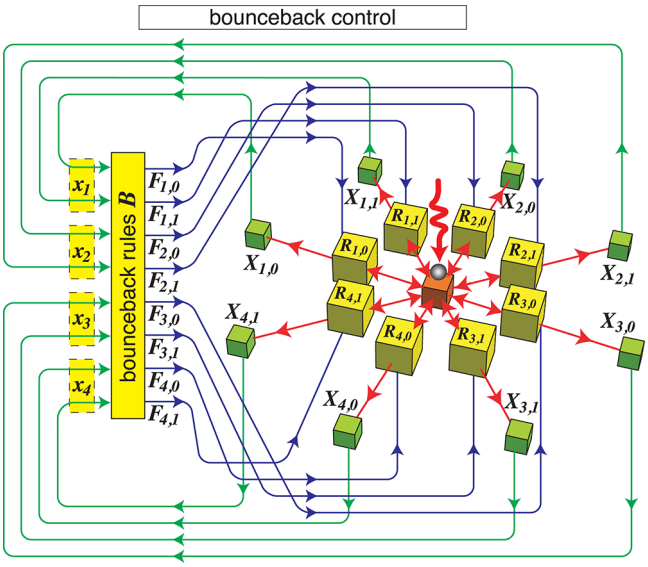

Figure 5. Data-flow diagram of the amoeba-inspired nanoarchitectonic computer.

that receive optical energy from QD_S, where the label (i,v) indicates that value $v \in \{0, 1\}$ is assigned to variable x_i ($i \in I = \{1, 2,..., N\}$) (i.e., $x_i = v$). When the exciton in QD_S is transferred to $QD_{i,v}$ and subsequently radiation is observed at a discrete time step t, we write this status as $R_{i,v}(t) = 1$, whereas $R_{i,v}(t) = 0$ indicates that no radiation occurs. When state-filling stimulation is applied to $QD_{i,v}$, we denote this status as $F_{i,v}(t) = 1$, whereas $F_{i,v}(t) = 0$ denotes no state filling. Thus, radiation $R_{i,v}(t) = 1$ occurs with a probability that depends on the state-filling stimulation $F_{i,v}(t)$ as follows:

$$R_{i,v}(t) = \begin{cases} 1 & (\text{with probability } p_{i,v}^+(t) \text{ if } F_{i,v}(t) = 1) \\ 1 & (\text{with probability } p_{i,v}^-(t) \text{ if } F_{i,v}(t) = 0) \\ 0 & (\text{otherwise}) \end{cases} \quad (5)$$

Figure 4 shows the dependence of the radiation probabilities of non-state-filled and state-filled $QD_{i,v}$'s, $p_{i,v}^-(t)$, and $p_{i,v}^+(t)$ on the number of all state-filled $QD_{j,u}$'s (i.e., $\Sigma_{j,u}F_{j,u}(t)$).

Each radiation event $R_{i,v}$ is accumulated by a newly introduced variable $X_{i,v} \in \{-1, 0, 1\}$ as follows:

$$X_{i,v}(t+1) = \begin{cases} X_{i,v}(t) + 1 & (\text{if } R_{i,v}(t) = 1 \text{ and } X_{i,v}(t) < 1) \\ X_{i,v}(t) - 1 & (\text{if } R_{i,v}(t) = 0 \text{ and } X_{i,v}(t) > -1) \\ X_{i,v}(t) & (\text{otherwise}) \end{cases} \quad (6)$$

Equation 6 can be implemented either physically or digitally; the values of $X_{i,v}$ can be stored either by some additional QDs or by some external control unit, as illustrated in Figures 5 and 1b, respectively. At each step t, the system transforms a configuration $X = (X_{1,0}, X_{1,1}, X_{2,0}, X_{2,1},..., X_{N,0}, X_{N,1})$ into an assignment $x = (x_1, x_2,..., x_N)$ as follows

$$x_i(t) = \begin{cases} 0 & (\text{if } X_{i,0}(t) = 1 \text{ and } X_{i,1}(t) \le 0) \\ 1 & (\text{if } X_{i,0}(t) \le 0 \text{ and } X_{i,1}(t) = 1) \\ x_i(t-1) & (\text{otherwise}) \end{cases} \quad (7)$$

where $x_i(0) =$ undefined for all i.

dx.doi.org/10.1021/la400301p | Langmuir XXXX, XXX, XXX–XXX

Bounceback Control Dynamics. The state-filling stimulations $F_{i,v}$ are updated synchronously according to the following dynamics

$$F_{i,v}(t+1) = \begin{cases} 1 & (\text{if } \exists\ (P, Q) \in B(\ \forall\ (j, u) \in P(X_{j,u}(t) = 1) \\ & \quad \text{and } (i, v) \in Q)) \\ 0 & (\text{otherwise}) \end{cases} \tag{8}$$

where B is a set of bounceback rules to be explained in this section. Each element (P, Q) in B implies the following statement: if all of the $X_{j,u}$'s specified by P are positive at t, then stimulate all $QD_{i,v}$'s specified by Q to inhibit their radiation at $t + 1$. Stated simply, if $x_j = u$, then x_i should not be v.

To see the meaning of the bounceback rules, let us consider the example formula ϕ_{ex}, which is shown in Figure 6a. To satisfy this formula for $\phi_{ex} = 1$, we should make every clause true because all clauses are connected by ∧. Suppose, for example, that the system tried to assign $x_1 = 0$ (i.e., $X_{1,0}(t) = 1$), as indicated by the red broken circle in Figure 6b. Now let us focus on the first clause $(x_1 \vee \neg x_2)$ in ϕ_{ex}. To make this clause true, if $x_1 = 0$ then x_2 should not be 1. Therefore, we apply state-filling stimulation $F_{2,1}(t + 1) = 1$ to inhibit the radiation $R_{2,1}(t + 1)$ of $QD_{2,1}$, as indicated by the blue broken circle. However, because x_3 in the third clause $(x_1 \vee x_3)$ should not be 0, we apply $F_{3,0}(t + 1) = 1$ (the blue dotted circle). In addition, we apply $F_{1,1}(t + 1) = 1$ (the blue solid circle) because if $x_1 = 0$ then obviously x_1 should not be 1. Likewise, the set of all bounceback rules B is determined by scanning all clauses in ϕ_{ex}, as shown in Table 1.

We formally define the set B = INTRA∪INTER∪CONTRA in what follows. INTRA forbids each variable i to take two values 0 and 1 simultaneously:

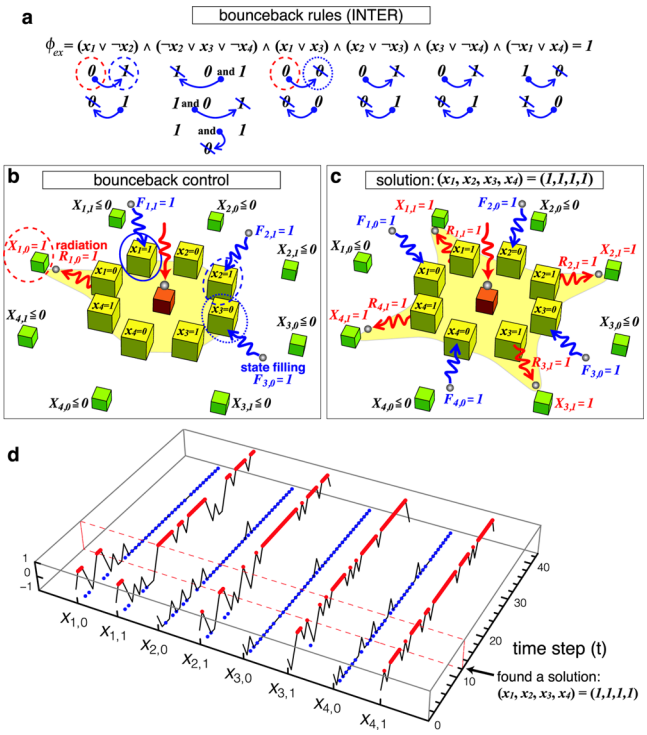

Figure 6. Bounceback control dynamics. (a) All bounceback rules in INTER for ϕ_{ex}. (b) Bounceback control applies state-filling stimulations $F_{1,1}(t + 1) = F_{2,1}(t + 1) = F_{3,0}(t + 1) = 1$ if $X_{1,0}(t) = 1$. (c) Configuration $X = (0, 1, 0, 1, 0, 1, 0, 1)$, which represents a solution $(x_1, x_2, x_3, x_4) = (1, 1, 1, 1)$. (d) Simulated time evolution. Red and blue dots indicate $X_{i,v}(t) = 1$ and $F_{i,v}(t) = 1$, respectively.

Table 1. All Bounceback Rules for ϕ_{ex}

B	P	Q
INTRA	{(1, 0)}	{(1, 1)}
	{(1, 1)}	{(1, 0)}
	{(2, 0)}	{(2, 1)}
	{(2, 1)}	{(2, 0)}
	{(3, 0)}	{(3, 1)}
	{(3, 1)}	{(3, 0)}
	{(4, 0)}	{(4, 1)}
	{(4, 1)}	{(4, 0)}
INTER	{(2, 1)}	{(1, 0)}
	{(1, 0)}	{(2, 1)}
	{(3, 0), (4, 1)}	{(2, 1)}
	{(2, 1), (4, 1)}	{(3, 0)}
	{(2, 1), (3, 0)}	{(4, 1)}
	{(3, 0)}	{(1, 0)}
	{(1, 0)}	{(3, 0)}
	{(3, 1)}	{(2, 0)}
	{(2, 0)}	{(3, 1)}
	{(4, 1)}	{(3, 0)}
	{(3, 0)}	{(4, 1)}
	{(4, 0)}	{(1, 1)}
	{(1, 1)}	{(4, 0)}
CONTRA	{(1, 1), (3, 0)}	{(1, 1), (3, 0)}
	{(1, 0), (2, 0)}	{(1, 0), (2, 0)}
	{(1, 0), (3, 1)}	{(1, 0), (3, 1)}
	{(2, 1), (4, 0)}	{(2, 1), (4, 0)}
	{(2, 0), (4, 1)}	{(2, 0), (4, 1)}
	{(3, 0), (4, 0)}	{(3, 0), (4, 0)}
	{(1, 1), (2, 1), (3, 0)}	{(1, 1), (2, 1), (3, 0)}
	{(2, 0), (2, 1), (4, 1)}	{(2, 0), (2, 1), (4, 1)}
	{(3, 0), (3, 1), (4, 1)}	{(3, 0), (3, 1), (4, 1)}

$$\text{INTRA} = \{(\{(i, v)\}, \{(i, 1 - v)\}) \mid i \in I \wedge v \in \{0, 1\}\} \tag{9}$$

Each clause $c = x_j^* \vee x_k^* \vee x_l^*$ in ϕ is represented as a set $C = \{j^*, k^*, l^*\}$ with its literals x_i^* mapped to $i^* = i$ if $x_i^* = x_i$ and to $-i$ otherwise, and the formula ϕ is expressed equivalently by a set Φ, which includes all of the clauses as their elements. The example formula ϕ_{ex} is transformed to $\Phi_{ex} = \{\{1, -2\}, \{-2, 3, -4\}, \{1, 3\}, \{2, -3\}, \{3, -4\}, \{-1, 4\}\}$. For each C in Φ and each variable i in C, INTER blocks the radiation [either $R_{i,0}(t + 1)$ or $R_{i,1}(t + 1)$] that makes c false

$$\text{INTER} = \{(P, \{(i, 0)\}) \mid i \in C \wedge C \in \Phi\} \cup \{(P, \{(i, 1)\}) \mid -i \in C \wedge C \in \Phi\} \tag{10}$$

where $P = \{(j, 0) \mid j \in C \wedge j \neq i\} \cup \{(j, 1) \mid -j \in C \wedge j \neq i\}$. Some rules in INTER may imply that neither 0 nor 1 can be assigned to a variable. To avoid this contradiction, for each variable i, we build CONTRA by checking all of the relevant rules in INTER:

$$\text{CONTRA} = \{(P \cup P', P \cup P') \mid i \in I \wedge (P, \{(i, 0)\}) \in \text{INTER} \wedge (P', \{(i, 1)\}) \in \text{INTER}\} \tag{11}$$

Before the computation, B is obtained in a polynomial time of $O(NM)$ by generating all of the bounceback rules in INTRA, INTER, and CONTRA according to the above procedures.

Note that the system can be stabilized if the following condition holds for all (i, v): if $X_{i,v}(t) = 1$ then $F_{i,v}(t) = 0$ or if $X_{i,v}(t) \leq 0$ then $F_{i,v}(t) = 1$. When this condition is not met, the system cannot be stabilized. Indeed, if $X_{i,v}(t) = 1$ and $F_{i,v}(t) = 1$, then radiation in $QD_{i,v}$ is likely to be inhibited as $R_{i,v}(t + 1) = 0$; consequently, $X_{i,v}(t + 2) = 0$. However, if $X_{i,v}(t) \leq 0$ and $F_{i,v}(t) = 0$, then radiation $R_{i,v}(t + 1) = 1$ is likely to be promoted to facilitate $X_{i,v}(t + 2) = 1$. These changes in the sign of $X_{i,v}$ make the system unstable. We designed the bounceback rules so that only satisfying assignments can be stabilized. This implies

dx.doi.org/10.1021/la400301p | Langmuir XXXX, XXX, XXX−XXX

that if a configuration X represents a solution then X can be maintained for the longest duration and thus occurs with the highest frequency when the system evolves for a sufficiently large number of iteration steps.

AmoebaSATnano and WalkSAT. Our numerical calculation method for simulating the amoeba-inspired computing paradigm can be used as an algorithm for solving SAT. We call this algorithm AmoebaSATnano. We evaluate the performance of AmoebaSATnano in comparison with that of the best-studied stochastic search algorithm called WalkSAT, which finds a solution with a reasonably large probability after a fairly small number of iterations.[34]

WalkSAT starts from a randomly chosen assignment $x = (x_1, x_2,..., x_N)$. At each iteration, by checking whether each clause in ϕ is satisfied by the current assignment x, WalkSAT randomly chooses one of the unsatisfied clauses and satisfies it by flipping one of its variables chosen at random (i.e., $0 \rightarrow 1$ and $1 \rightarrow 0$). This routine is iterated until x satisfies ϕ or we run out of time. Schöning estimated the average number of iterations that WalkSAT required to find a solution to a 3-SAT as an exponential function of $(^4/_3)^N \mathrm{poly}(N)$.[34] WalkSAT is one of the fastest algorithms.[35]

RESULTS

The computation of AmoebaSATnano starts at $X_{i,v}(0) = R_{i,v}(0) = F_{i,v}(0) = 0$ for all (i, v), and the time evolution of the system is simulated by updating eqs 5, 6, and 8 iteratively. Figure 6d shows that the system successfully found the solution of the example formula ϕ_{ex} at $t = 12$, which is represented by the configuration shown in Figure 6c. We can confirm that $X = (0, 1, 0, 1, 0, 1, 0, 1)$, which represents the solution $(x_1, x_2, x_3, x_4) = (1, 1, 1, 1)$ that is observed most frequently after $t = 12$.

We compared the performance of AmoebaSATnano and WalkSAT for benchmark SAT instances, which are provided to the public by SATLIB online.[36,37] We used a family of 3-SAT instance distributions, Uniform Random-3-SAT, which was obtained by randomly generating three-literal conjunctive normal form formulas. The hardness of a 3-SAT has been shown to be maximal when the ratio between the number of variables N and the number of clauses M is set at the phase-transition region around $M/N = 4.26$.[38,39] We chose 100 instances each from each of the test sets uf75−325 and uf100−430, which took satisfiable $N = 75 - M = 325$ and $N = 100 - M = 430$ formulas from the most difficult regions, $M/N \approx 4.333$ and $M/N = 4.3$, respectively.

For each instance, we conducted 500 trials consisting of Monte Carlo simulations to obtain the average number of iterations (time steps t) required to find a solution. Figure 7 shows that in almost all instances AmoebaSATnano found a solution more quickly than WalkSAT. In particular, AmoebaSATnano outperformed WalkSAT more significantly as N increased.

DISCUSSION AND CONCLUSIONS

We demonstrate that photoexcitation transfer phenomena in a QDs system mediated by optical near-field interactions can be used to solve SAT. Our amoeba-inspired computing paradigm is fundamentally different from conventional optical computing or optical signal processing, which are limited by the properties of propagating light. Our paradigm also differs from the quantum computing paradigm, which exploits a superposition of all possible states to produce a correct solution. This is because our paradigm exploits both coherent and dissipative processes. In fact, optical-near-field-mediated photoexcitation transfer is a coherent process, suggesting that an exciton could be transferred to all possible destination QD_L's via a resonance

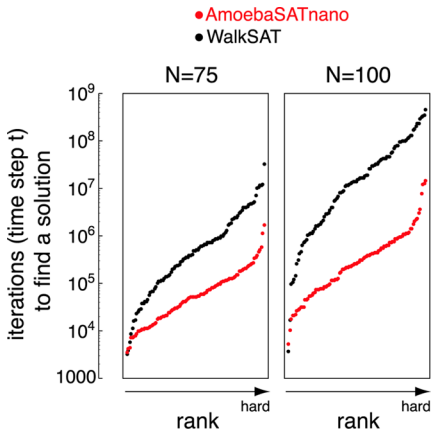

Figure 7. Performance comparison between our AmoebaSATnano (red) and the well-known WalkSAT (black) for benchmark 3-SAT instances of $N = 75$ and 100. Each point indicates the number of iterations required to find a solution for each instance, averaged over 500 trials. For each algorithm and each N, we evaluated 100 points (instances) and ranked (sorted) all of the points from easiest to most difficult (requiring the largest number of iterations). The results are compared on a logarithmic scale, which implies that AmoebaSATnano has a significant advantage over WalkSAT.

energy level, but such a coherent interaction produces a unidirectional transfer by an energy dissipation process occurring in QD_L. A strength of our paradigm is that photoexcitation transfer is 10^4 times more energy efficient than conventional electrically wired bit-flip circuits.[28]

An important issue that we should address to implement our paradigm experimentally is a means of introducing the bounceback control dynamics; at each iteration, the control dynamics should store the values of $X_{i,v}(t)$ by detecting the radiation values $R_{i,v}(t)$, determine the state-filling stimulations $F_{i,v}(t + 1)$ according to the set of bounceback rules B, and apply these stimulations to $QD_{i,v}$'s, as shown in Figure 5. An external approach would be to use an external control unit such as a combination of a PC with a projector, as we did for the amoeba-based computing (Figure 1b). However, the external control unit may impose additional energy costs and may limit the processing speed of our paradigm. However, an internal approach could implement the control dynamics using additional QDs without introducing the external control unit. It may be possible to embed the counterpart of the external control unit in the arrangement of QDs because the bounceback rules are expressed by combining elementary logical operations and these logical operations have already been implemented experimentally using several QD systems.[26]

Because SAT is NP-complete, a powerful SAT solver is useful for a broad spectrum of applications in artificial intelligence, information security, and bioinformatics. We demonstrated that, for benchmark 3-SAT instances chosen from the most difficult region, our paradigm found a solution much faster than did the conventionally known fastest algorithm. We believe that the origin of the high performance of our paradigm will be attributed to interactions among the QDs. At each iteration, the conventional algorithm flips a single state without implementing any interaction among the variables. In contrast, our paradigm updates at most $2N$ states through a large number of interactions among the QDs, which exchange information on stimulated experiences via the bounceback control dynamics. This difference in the number of interactions might produce a

dx.doi.org/10.1021/la400301p | Langmuir XXXX, XXX, XXX−XXX

huge difference in the computing power.[1] This discussion would be supported by the fact that our paradigm became more advantageous as N increased.

Putting these facts together, this Article paves the way for applying nanometer-scale optical near-field interactions to develop novel low-energy-use highly versatile powerful computers. We believe that our amoeba-inspired computing paradigm presents a promising direction for nanoarchitectonics, which harnesses novel functionalities in the interactions among nanoscale elements.

AUTHOR INFORMATION

Corresponding Author

*E-mail: masashi.aono@elsi.jp.

Notes

The authors declare no competing financial interest.

REFERENCES

(1) Conrad, M. The Price of Programmability. In *The Universal Turing Machine: A Half-Century Survey*; Rolf, H., Ed.; Springer-Verlag: Wien, Austria, 1994; pp 261−281.

(2) Berger, B.; Leighton, T. Protein Folding in the Hydrophobic-Hydrophilic (HP) Model is NP-Complete. *J. Comput. Biol.* **1998**, *5*, 27−40.

(3) Garey, M. R.; Johnson, D. S. *Computers and Intractability: A Guide to the Theory of NP-Completeness*, W.H. Freeman and Co.: New York, 1979.

(4) Rozenberg, G., Bäck, T., Kok, J., Eds. *Handbook of Natural Computing*; Springer-Verlag: New York, 2012.

(5) *International Technology Roadmap for Semiconductors*. Emerging Research Devices, 2009.

(6) Hopfield, J. J.; Tank, D. W. Computing with Neural Circuits: A Model. *Science* **1986**, *233*, 625−633.

(7) Holland, J. H. *Adaptation in Natural and Artificial Systems*, 2nd ed.; MIT Press: Cambridge, MA, 1992.

(8) Dorigo, M.; Maniezzo, V.; Colorni, A. Ant System: Optimization by a Colony of Cooperating Agents. *IEEE Trans. Syst. Man Cybern. B* **1996**, *26*, 29−41.

(9) Poli, R.; Kennedy, J.; Blackwell, T. Particle Swarm Optimization. *Swarm Intell.* **2007**, *1*, 33−57.

(10) Nakagaki, T.; Yamada, H.; Toth, A. Intelligence: Maze-Solving by an Amoeboid Organism. *Nature* **2000**, *407*, 470.

(11) Tero, A.; Takagi, S.; Saigusa, T.; Ito, K.; Bebber, D. P.; Fricker, M. D.; Yumiki, K.; Kobayashi, R.; Nakagaki, T. Rules for Biologically Inspired Adaptive Network Design. *Science* **2010**, *327*, 439−442.

(12) Takamatsu, A.; Tanaka, R.; Yamada, H.; Nakagaki, T.; Fujii, T.; Endo, I. Spatiotemporal Symmetry in Rings of Coupled Biological Oscillators of Physarum Plasmodial Slime Mold. *Phys. Rev. Lett.* **2001**, *87*, 078102.

(13) Takagi, S.; Ueda, T. Emergence and Transitions of Spatiotemporal Patterns in Thickness Oscillation by the Plasmodium of the True Slime Mold Physarum Polycephalum. *Phys. D* **2008**, *237*, 420−427.

(14) Aono, M.; Gunji, Y.-P. Beyond Input-output Computings: Error-driven Emergence with Parallel Non-Distributed Slime Mold Computer. *BioSystems* **2003**, *71*, 257−287.

(15) Aono, M.; Hara, M.; Aihara, K. Amoeba-Based Neurocomputing with Chaotic Dynamics. *Commun. ACM* **2007**, *50*, 69−72.

(16) Aono, M.; Hirata, Y.; Hara, M.; Aihara, K. Amoeba-based Chaotic Neurocomputing: Combinatorial Optimization by Coupled Biological Oscillators. *New Gener. Comput.* **2009**, *27*, 129−157.

(17) Zhu, L.; Aono, M.; Kim, S.-J.; Hara, M. Amoeba-Based Computing for Traveling Salesman Problem: Long-Term Correlations between Spatially Separated Individual Cells of Physarum Polycephalum. *BioSystems* **2013**, *112*, 1−10.

(18) Zhu, L.; Aono, M.; Kim, S.-J.; Hara, M. Problem-Size Scalability of Amoeba-Based Neurocomputer for Traveling Salesman Problem. *Proc. NOLTA* **2011**, 108−111.

(19) Aono, M.; Kim, S.-J.; Zhu, L.; Naruse, M.; Ohtsu, M.; Hori, H.; Hara, M. Amoeba-Inspired SAT Solver. *Proc. NOLTA* **2012**, 586−589.

(20) Naruse, M.; Miyazaki, T.; Kawazoe, T.; Sangu, S.; Kobayashi, K.; Kubota, F.; Ohtsu, M. Nanophotonic Computing Based on Optical Near-Field Interactions Between Quantum Dots. *IEICE Trans. Electron. E88-C* **2005**, 1817−1823.

(21) Naruse, M.; Aono, M.; Kim, S.-J.; Kawazoe, T.; Nomura, W.; Hori, H.; Hara, M.; Ohtsu, M. Spatiotemporal Dynamics in Optical Energy Transfer on the Nanoscale and Its Application to Constraint Satisfaction Problems. *Phys. Rev. B* **2012**, *86*, 125407.

(22) Ohtsu, M.; Kawazoe, T.; Yatsui, T.; Naruse, M. Single-Photon Emitter Using Excitation Energy Transfer between Quantum Dots. *IEEE J. Sel. Top. Quantum Electron.* **2009**, *14*, 1404−1417.

(23) Kawazoe, T.; Kobayashi, K.; Akahane, K.; Naruse, M.; Yamamoto, N.; Ohtsu, M. Demonstration of Nanophotonic NOT Gate Using Near-Field Optically Coupled Quantum Dots. *Appl. Phys. B: Laser Opt.* **2006**, *84*, 243−246.

(24) Yatsui, T.; Sangu, S.; Kawazoe, T.; Ohtsu, M.; An, S. J.; Yoo, J.; Yi, G.-C. Nanophotonic Switch Using ZnO Nanorod Double-Quantum-Well Structures. *Appl. Phys. Lett.* **2007**, *90*, 223110.

(25) Nomura, W.; Yatsui, T.; Kawazoe, T.; Naruse, M.; Ohtsu, M. Structural Dependency of Optical Excitation Transfer via Optical Near-Field Interactions between Semiconductor Quantum Dots. *Appl. Phys. B: Laser Opt.* **2010**, *100*, 181−187.

(26) Kawazoe, T.; Ohtsu, M.; Aso, S.; Sawado, Y.; Hosoda, Y.; Yoshizawa, K.; Akahane, K.; Yamamoto, N.; Naruse, M. Two-Dimensional Array of Room-Temperature Nanophotonic Logic Gates Using InAs Quantum Dots in Mesa Structures. *Appl. Phys. B: Laser Opt.* **2011**, *103*, 537−546.

(27) Akahane, K.; Yamamoto, N.; Tsuchiya, M. Highly Stacked Quantum-Dot Laser Fabricated Using a Strain Compensation Technique. *Appl. Phys. Lett.* **2008**, *93*, 041121.

(28) Naruse, M.; Hori, H.; Kobayashi, K.; Holmström, P.; Thylén, L.; Ohtsu, M. Lower Bound of Energy Dissipation in Optical Excitation Transfer via Optical Near-Field Interactions. *Opt. Express* **2010**, *18*, A544−A553.

(29) Ohtsu, M.; Kobayashi, K.; Kawazoe, T.; Yatsui, T.; Naruse, M. *Principles of Nanophotonics*; Taylor and Francis: Boca Raton, FL, 2008.

(30) Itoh, T.; Furumiya, M.; Ikehara, T.; Gourdon, C. Size-dependent Radiative Decay Time of Confined Excitons in CuCl Microcrystals. *Solid State Commun.* **1990**, *73*, 271−274.

(31) Carmichael, H. J. *Statistical Methods in Quantum Optics 1*; Springer-Verlag: Berlin, 1999.

(32) Nomura, W.; Yatsui, T.; Kawazoe, T.; Ohtsu, M. The Observation of Dissipated Optical Energy Transfer between CdSe Quantum Dots. *J. Nanophotonics* **2007**, *011591*, 1−7.

(33) Kim, S.-J.; Aono, M.; Hara, M. Tug-of-War Model for the Two-Bandit Problem: Nonlocally-Correlated Parallel Exploration via Resource Conservation. *BioSystems* **2010**, *101*, 29−36.

(34) Schöning, U. A Probabilistic Algorithm for k-SAT and Constraint Satisfaction Problems. *Proceedings of the 40th Symposium on the Foundations of Computer Science*, 1999, pp 410−414.

(35) Iwama, K.; Tamaki, S. Improved Upper Bounds for 3-SAT.*Proceedings of the 15th Symposium on Discrete Algorithms*, 2004, pp 328−328

(36) http://www.cs.ubc.ca/~hoos/SATLIB/benchm.html.

(37) Hoos, H.; H., Stutzle, T. SATLIB: An Online Resource for Research on SAT. *Proc. SAT* **2000**, 283−292.

(38) Mitchell, D.; Selman, B.; Levesque, H. Hard and Easy Distributions of SAT Problems. *Proc. AAAI* **1992**, 459−465.

(39) Kirkpatrick, S.; Selman, B. Critical Behavior in the Satisfiability of Random Boolean Expressions. *Science* **1994**, *264*, 1297−1301.